Korean J. Chem. Eng., 35(4), 964-973 (2018)
DOI: 10.1007/s11814-017-0354-0

pISSN: 0256-1115
eISSN: 1975-7220

Anti-fouling characteristic of carbon nanotubes hollow fiber membranes by filtering natural organic pollutants

Yue Yang, Sen Qiao†, Ruofei Jin, Jiti Zhou, and Xie Quan†

Key Laboratory of Industrial Ecology and Environmental Engineering (Ministry of Education, China), School of Environmental Science and Technology, Dalian University of Technology, Dalian 116024, P. R. China
(*Received 22 September 2017 • accepted 26 December 2017*)

Abstract−Membrane fouling is a universal problem for conventional membrane filtration that usually causes a deterioration in membrane performance. We used electro-assisted carbon nanotubes hollow fiber membranes (CNTs-HFMs) to investigate the anti-fouling properties using natural organic pollutants. Benefiting from the electro-assistance, the permeation flux of humic acid solution using CNTs-HFMs was 190.20 L/(m^2·h·bar), which was about 1.5- and 4.4-times higher than those of CNTs-HFMs without electro-assistance and traditional polyvinylidene fluoride hollow-fiber membranes (PVDF-HFMs). And the permeation fluxes of bovine serum albumin, sodium alginate and supernatant of anaerobic bioreactor also presented similar results. The average COD removal rate of CNTs-HFMs (66.8%) at −1.0 V was higher than that of CNTs-HFMs without electro-assistance and PVDF-HFMs, which can be attributed to the formation of electrostatic repulsive force. It could reduce the deposition of pollutants on membrane surface under electro-assistance.

Keywords: Carbon Nanotubes Hollow Fiber Membranes, Membrane Fouling, Natural Organic Pollutants, Electrochemical Effects, COD Removal

INTRODUCTION

As an efficient treatment system, anaerobic membrane bioreactors (AnMBR) can overcome the drawbacks of the conventional anaerobic biological treatment, such as sludge loss and large occupation area, thus becoming a research hotspot [1,2]. However, membrane fouling, as the main obstacle in its operation, can lead to higher transmembrane pressure, lower effluent flux and more operational complexity [3]. Generally, membrane fouling is caused by interaction between the membrane materials and the substance in the filtrate. The latter includes substrate components, cells, cell debris, and microbial metabolites such as soluble microbial products (SMP) and extracellular polymeric substances (EPS) [4,5]. Among them, SMP and EPS play a very important role in membrane fouling, which is prevalent in the interior and surface of biomass flocs, consisting of the main ingredient of pollutants. SMP and EPS are polymers of some macromolecules such as polysaccharides, proteins and nucleic acids, most of which have negative charges [6]. Recently, many studies have identified SMP and EPS as the most significant biological factor responsible for membrane fouling [7], since they can result in membrane pore blockage, mud cake layer and gel layer etc. [8-10].

The traditional fouling mitigation strategies can be divided into chemical and physical methods. However chemical cleaning will generally cause membrane material corrosion and destruction, and the residual chemical substances are also harmful to the microorganisms. While, physical technologies have low efficiency, or have some dead ends [10-13]. Over the last few years, many significant membrane anti-fouling strategies have been developed, mainly focusing on membrane surface modification and membrane materials improvement in order to reduce the interaction between membrane materials and microorganisms or their secretions and further enhance the anti-fouling property. Among them, conductive materials modification on membrane surface or direct application as the membrane materials has shown great prospects since charge repelling action could prevent EPS attachment, and electrochemical action might degrade the attached pollutants on the membrane surface. Katuri et al. [14] used electrically conductive nickel-based hollow-fiber membranes (Ni-HFMs) as membrane filtration system to treat low organic strength solution. The experimental results showed that the membrane fouling at an applied voltage 0.9 V was obviously much lighter than that applying 0.5 V, because the gas bubble formation could provide a means of scouring (self-cleaning) the surface of the membranes. Gunawan et al. [15] developed a novel water disinfection system consisting of silver nanoparticle/multiwalled carbon nanotubes (Ag/MWNTs) coated on a polyacrylonitrile (PAN) hollow fiber membrane to form new Ag/MWNTs/PAN hollow fiber membrane. And a lower level of membrane fouling was obtained through the presence of the Ag/MWNT disinfection layer, which effectively inhibited the growth of bacteria in the filtration module and prevented the formation of biofilm on the surface of the membrane. Wei et al. [16] used hollow fiber membranes based on carbon nanotubes at different voltage to form a voltage-gate, which could control specific ions transport. Then an efficient way reducing membrane fouling was demonstrated, which can control membrane pore clogged by charges particles.

†To whom correspondence should be addressed.
E-mail: qscyj@mail.dlut.edu.cn, quanxie@dlut.edu.cn

Table 1. Properties of the materials and analysis methods

Chemicals	Molecular formula	Purity (%)	Grade	Water solubility
Humic acid	$C_9H_9NO_6$	≥90.0	AR	Slightly soluble
Bovine serum albumin	$C_8H_{21}NOSi_2$	≥98.0	AR	Easily soluble
Sodium alginate	$(C_6H_7NaO_6)_n$	≥99.9	AR	Slightly soluble
N,N-Dimethylformamide	$HCON(CH_3)_2$	≥99.5	AR	Soluble
Polyvinyl Butyral	$C_{16}H_{28}O_5$	≥99.0	AR	Insoluble
Sulphuric acid	H_2SO_4	95.0-98.0	AR	Soluble
Nitric acid	HNO_3	≥65.0	AR	Soluble

Carbon nanotubes (CNTs) have been reported as a promising material for constructing membranes owing to their outstanding properties, including high surface area, high mechanical strength, excellent chemical inertness, and water-transport [17]. Because of the overlap and interpenetration of CNTs, as-constructed CNT membranes with mesh-like structures usually present numerous interconnected pores and high porosities (>70%) [18]. These properties further endow CNT membranes with a high flux even at a low operating pressure. Regarding the geometry of the membrane, hollow fibers have the highest surface area per volume ratio, which makes them very appealing because of the possibility of obtaining small membrane modules with large surface areas and thus achieving a small foot print [19]. Recently, carbon nanotube hollow fiber membranes (CNTs-HFMs) have been successful prepared to effectively combine the characteristics of CNTs and hollow structures [20,21]. Especially, CNTs exhibit encouraging electrochemical performances such as good conductivity. The electro-assisted CNTs-HFMs would present an outstanding anti-fouling capacity, because this fouling mitigation is ascribed to a static electric respelling force imposed by the electric field, which reduces the adsorption of negatively charged pollutants (such as SMP and EPS) onto the equally negatively charged membrane surface [22]. Moreover, the hydrophilicity of CNTs will definitely endow CNT-HFMs much higher pure water flux, which is also beneficial for the long-term operation and stability of MBRs. CNTs as one of the fine chemicals productions, have been applied widely in additives field, for example, plastic preparation [23], rubber synthesis [24] and paint synthesis [25].

In this study, we used multi-walled-carbon-nanotubes-(CNTs)-based conductive hollow fiber membranes (CNTs-HFM) to construct a novel filtration system. Four kinds of pollutants, such as humic acid (HA), bovine serum albumin (BSA), sodium alginate (SA) and supernatant of anaerobic bioreactor, were utilized as the test pollutants to explore the anti-fouling mechanisms of CNTs-HFMs. The degradation of organic pollutants and membrane fouling were studied to evaluate applied voltage on the performance of the system, which would provide some theoretical basis and technical support for membranes with the special electrochemical environment.

MATERIALS AND METHODS

1. Materials

PVDF-HFMs and the pristine multi-walled CNTs (purity >98%) were purchased from Hangzhou Haotian Membrane Technology Co., Ltd., China and Shenzhen Nanotech Port Co., Ltd., China, respectively. N,N-Dimethylformamide (DMF) was obtained from Xilong Chemical Company Co., Ltd., China. Polyvinyl butyral (PVB) and PVA were both purchased from Sinopharm Chemical Reagent Co., Ltd., China. Humic acid (HA), bovine serum albumin (BSA) and sodium alginate (SA) were obtained from Sigma-Aldrich Chemical Company, USA. Other chemicals, such as H_2SO_4 and HNO_3 were all analytical grade and supplied by Bench Chemicals (Tianjin, China). Finally, ultrapure water (resistivity >18 $M\Omega cm^{-1}$) produced by a purification system (Beijing Purkinje General Instrument Company Co., Ltd., China) was used in all experiments. More detailed properties of the materials are summarized in Table 1.

2. Preparation and Characterization of CNTs-HFMs and PVDF-HFMs

2-1. Preparation the CNTs-HFMs

The preparation procedures of CNTs-HFMs were based on wet-spinning technologies. Briefly, surface-functionalized CNTs and PVB were dispersed and dissolved in DMF to form a homogeneous spinning solution, then through a coaxial two capillary spinneret to obtain CNT/PVB hollow fibers. Subsequently, to get free-standing CNT hollow fiber membranes, the products were calcined in a flow of argon (40 sccm) at 600 °C for 2 h at a heating rate of 2 °C·min^{-1}. The last step was to soak membranes into 1% PVA for 4 h to change its toughness, then naturally dried at room temperature (20 °C) [21].

2-2. Morphologies of the CNTs-HFMs and PVDF-HFMs

The membrane surface was observed by SEM (FESEM, Hitachi S-8010) on a microscope with 1.0 nm resolution, and the microscope was operated at 5 kV. To obtain top view, the CNTs-HFMs were dried at room temperature (20 °C) and the PVDF-HFMs were sputter-coated with gold.

2-3. Interaction Force Among Membranes

The interaction force between the foultant and the membrane surface was measured by atomic force microscopy (AFM, Bruker Dimension Icon, Germany) and the force measurements were performed by SiN AFM probe modified with a colloid probe. The modified process was described as below [26,27]: Because carboxylic groups were the predominant function groups of humic acid, a carboxylic polystyrene micro-particle (So-Fe Biomedical Co., Ltd., China) was used to modify SiN probe. The micro-particles were 18 μm in diameter, and the surface charge was 200-300 μC/cm^2. A drop of micro-particle suspension was first spread on freshly carrying fragments and dried naturally. The carboxylic poly-

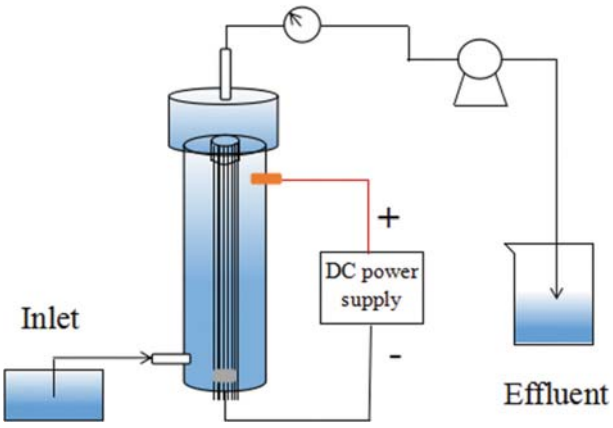

Fig. 1. Flow chart of CNTs-HFMs filtration reaction.

styrene micro-particle and the AFM probe was connected by epoxy glue. The whole process was operated under an optical microscope (YPN-400, Zhaoyi Optoelectronics Technology Co., Ltd., China) and all force measurements were conducted using the same colloid probe. To make the results more accurate, each sample was measured many times at different positions.

2-4. Pure Water Flux

Pure water flux was used to evaluate the permeability of the membranes. The filtration process was kept steady for at least 30 minutes at a constant pressure, and the time, pressure and pure water volume were recorded. The pure water flux was measured using a dead-end filtration device (Fig. 1) and calculated as in Eq. (1) [21]:

$$J = \frac{V}{A \cdot \Delta t} \quad (1)$$

where J is the permeation flux (L/m^2·h), V is the volume of the permeate (L), A is the membrane area (m^2) and Δt is the permeate collection interval (h). The flux recovery (F_r) is calculated by the following Eq. (2) [28]:

$$F_r(\%) = \left(\frac{J_{M,i}}{J_{M,1}}\right) \times 100 \quad (2)$$

where, $J_{M,1}$ is the initial flux of the membrane for natural organic pollutant water before the first cycle, $J_{M,i}$ is the membrane flux (after cleaning the membrane by clean water) for natural organic pollutant water after cycle i.

2-5. Contact Angles

Contact angle (θ) is the angle of gas, liquid and solid three-phase when micro-droplets are touching solid sample surface, which can characterize membrane hydrophilicity or hydrophobicity. In this study, contact angles of CNTs-HFMs and PVDF-HFMs were measured by automatic contact angle meter (SL200B, Kono Industrial Co., Ltd., USA); the liquid was ultrapure water.

2-6. Membrane Pore Size

Membrane pore size is another important indicator of membrane materials. The suitable pore size can hold up pollutants adequately, slow down the rate of fouling. Membrane pore sizes of CNTs-HFMs and PVDF-HFMs were measured by a pore size tester (POROLUX^{TM}1000, POROMETER, Germany); the total measurement range of this instrument was from 500 microns to 18 nm, and the wetting liquid was anhydrous ethanol.

3. Filtration Tests

In anti-fouling tests, a dead-end filtration device (Fig. 1) was used to investigate the anti-fouling capabilities of the membranes. The filtration experiments were all under 0.7 bar transmembrane pressure, and the PVDF-HFMs and CNTs-HFMs module used in this manuscript had an effective area of 0.001256 m^2 (0.0016 m×3.14×0.05 m×5 and 0.0004 m×3.14×0.1 m×10, respectively). HA (8 g/L), BSA (8 g/L), SA (4 g/L) and supernatant of anaerobic bioreactor were chosen as the target pollutants. Among them, the COD of supernatant of anaerobic bioreactor was average 305.7 mg/L, pH was approximately 7.0, polysaccharides concentration was 9.15 mg/L and protein concentration was 2.27 mg/L. When the flux decreased below 10 L/(m^2·h·bar), membrane materials were viewed as total blocked and the end of this running stage. Hydraulic cleaning (ultrasound for three minutes in pure water) was then conducted. The cleaned membrane materials were used to filtrate the same pollutants once again to evaluate the flux recover capacity for the next running stage. Generally, three stages were carried out for each kind of pollutants.

Similarly, when "−1.0 V" voltage [14] was applied on CNTs-HFMs, HA (8 g/L), BSA (8 g/L) and supernatant of anaerobic bioreactor were utilized as the pollutants to investigate the anti-fouling effect of CNTs-HFMs with and without voltage application. After filtration experiments, COD removal, SEM and AFM observations were performed for deeply understanding the relationship between the coupling effect of membrane with voltage and anti-fouling performance.

RESULTS AND DISCUSSION

1. Characterization of the CNTs-HFMs and PVDF-HFMs

1-1. Morphologies and Surface Pore Size

SEM images indicated that the CNTs-HFMs had smooth outer surface without any crack (Fig. 2(a)), the same as PVDF-HFMs (Fig. 2(b)). It can reduce the fouling level of membrane pore blockage since the insoluble contaminants were not easily to block the smooth surface [29-31]. And the CNTs-HFMs had random pore structure without any obvious structural collapse, characterized by an interwoven network structure (Fig. 2(c)) contrasting with PVDF-HFMs (Fig. 2(d)). This special pore structure endowed the CNTs-HFMs with a higher flux (shown in part 3.1.2) up to eight-times than that of PVDF-HFMs at the same pressure (Table 2). Moreover, it can also prevent membranes from being deeply pore blocked, thus reducing the membrane fouling. And based on the cross section observation, CNTs-HFMs and PVDF-HFMs had uniform outer/inner diameters 400/240 μm (Fig. 2(e)) and 1,600/690 μm (Fig. 2(f)), respectively.

Another property of CNTs membrane was a relatively larger surface pore size (support information Fig. S1) than that of PVDF membranes, which were about 428.6 nm and 304.2 nm, respectively. Some studies reported that surface pore size had a direct impact on membrane fouling, and the influence of pore size on membrane fouling strongly depends on the feed solution characteristics, in particular, particle size distribution [32]. Even the small

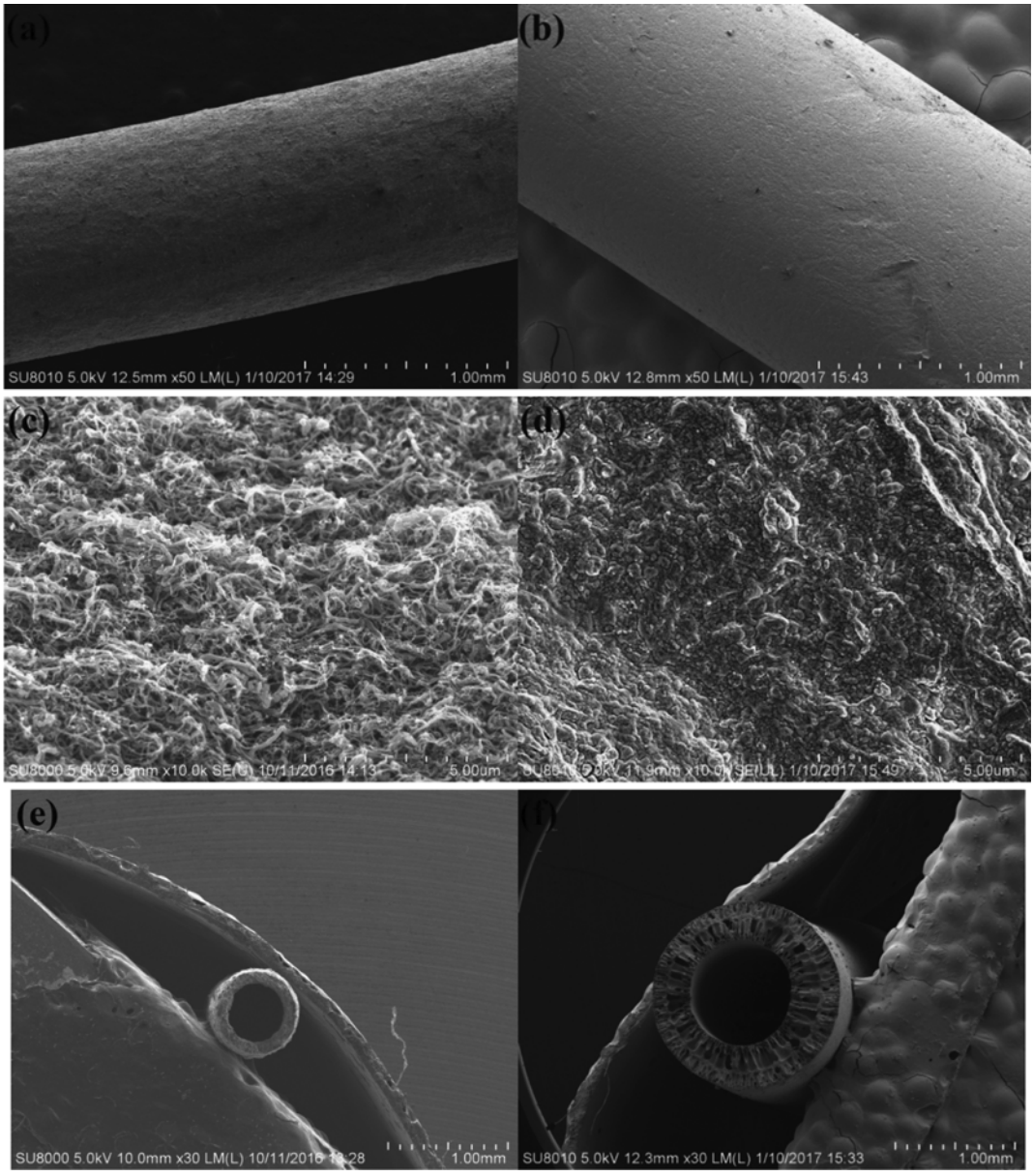

Fig. 2. SEM images of modified CNTs-HFMs surface (a), (c); PVDF-HFMs surface (b), (d); Cross section of CNTs-HFMs (e); Cross section of PVDF-HFMs (f).

surface pore size property can intercept substances with small particle size, and it can easily lead to serious membrane fouling and low flux.

1-2. Pure Water Flux

Flux is an important indicator for membrane performance. A higher flux can meet effluent needs with a lower pressure, which could reduce the damage potential to the membrane materials [33]. To compare the filtration capacity of both membranes, the pure water flux of the two kinds of membranes was monitored at different constant pressure using dead-end filtration devices (Fig. 1 and Table 2). The results proved that the pure water fluxes of CNT-HFMs were always higher than those of PVDF-HFMs. Even at the low pressure of 0.2 bar, the pure water fluxes of CNTs-HFMs climbed up to 145.49 L/m^2·h, about 6.6-fold as high as that of PVDF-HFMs. Later, when the pressure increased to 0.7 bar, the pure water fluxes of the CNTs-HFMs and PVDF-HFMs reached

Table 2. Pure water flux of at different pressure

Pressure (bar)	CNTs-HFMs (L/m^2·h)	PVDF-HFMs (L/m^2·h)
0.1	44.46	19.60
0.2	145.49	22.05
0.3	169.74	24.50
0.4	210.16	26.95
0.5	242.49	30.62
0.6	286.95	35.52
0.7	339.49	44.10

339.49 L/m^2·h and 44.1 L/m^2·h, respectively. The former was nearly eight-times higher than that of PVDF-HFMs. This phenomenon can be explained by two aspects. First, hydrophilicity (contact angle of 75.36°) made membranes easily wetted by water and then consequently available for water transport across the membranes. Second, the interwoven network of CNTs and random pore structure (see the SEM images in Fig. 2(c), (d)) resulted in a high porosity per unit area of the CNTs-HFMs, which can endow CNTs membranes with high-throughput property (339.49 L/m^2·h).

1-3. Contact Angles

Hydrophilicity/hydrophobicity can affect filtration performance and fouling levels, because the pore channels of hydrophobic membranes cannot be wetted by water, and consequently are unavailable for water transport across the membranes. Moreover, a water film cannot be formed on the hydrophobic membrane surface, which can prevent the insoluble contaminants from blocking the pore channels seriously [34,35]. Thus, hydrophilicity plays a vital role in membranes anti-fouling performance. As shown in Fig. 3, the contact angles of the CNTs-HFMs and PVDF-HFMs were 75.36° and 102.26°, respectively. And then water droplet on the CNTs-HFMs was absorbed completely only after 3,500 ms; however, the contact angle of PVDF-HFMs had only decreased by about 15° at the same period. These results implied that the hydrophobic CNTs after acidification had changed to hydrophilic.

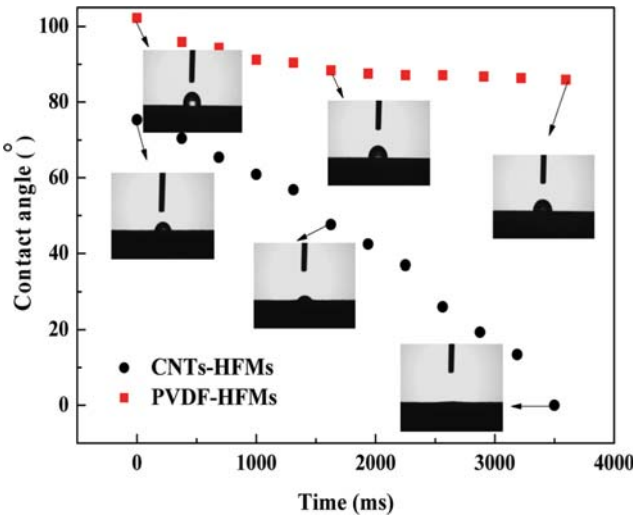

Fig. 3. The contact angles of CNTs-HFMs and PVDF-HFMs.

2. Anti-fouling Properties of the CNTs-HFMs

Fig. 4 depicts the flux variations of HA, BSA, SA and anaerobic bioreactor's supernatant pollutants. Although the CNTs-HFMs suffered flux decreasing during each stage, the special random pore channels and dense interwoven network structure made the initial flux much higher than that of PVDF. For HA filtration, the initial flux of PVDF-HFMs was 36.6 L/(m^2·h·bar). Water permeation flux through CNTs-HFMs was much improved (97.36 L/(m^2·h·bar)) because of its hydrophilic functional groups. More-

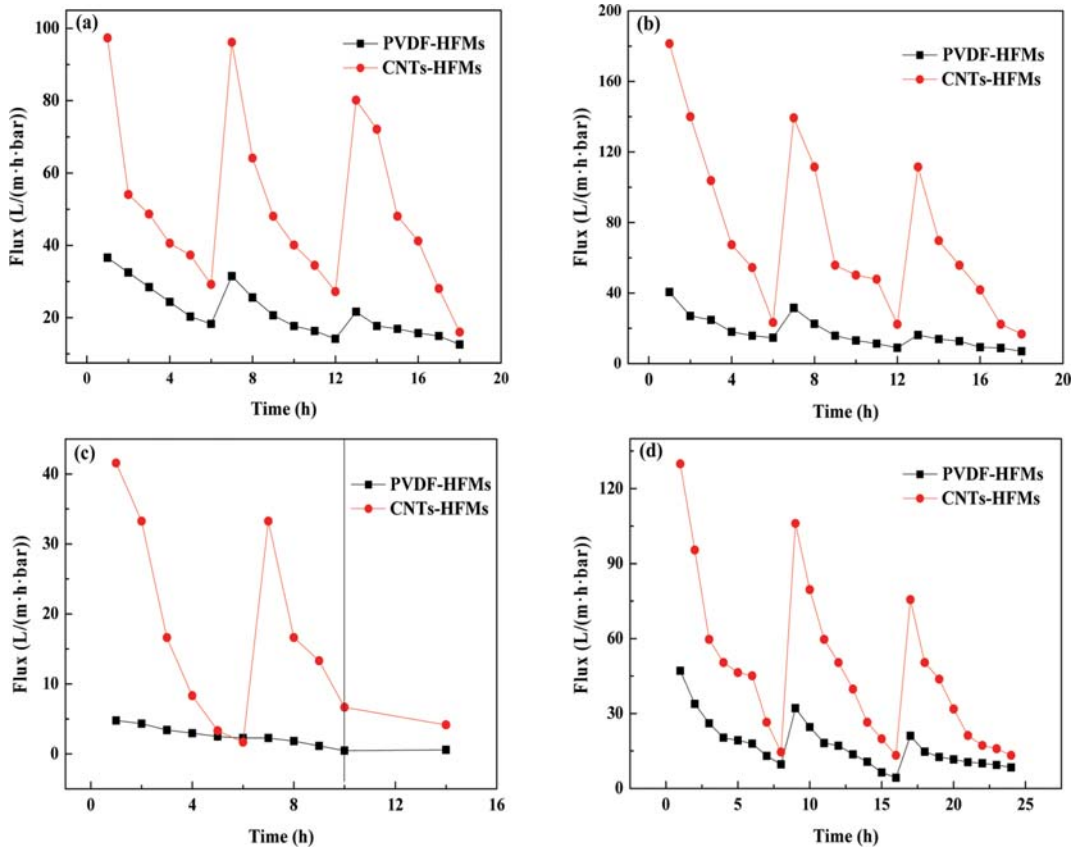

Fig. 4. The experiment of flux recovery: (a) 8 g/L Humic acid. (b) 8 g/L Bovine serum albumin. (c) 4 g/L Sodium alginate. (d) Supernatant of anaerobic bioreactor.

Table 3. The percent flux recovery of CNTs-HFMs and PVDF-HFMs by different pollutants at each stage

Pollutants	HA		BSA		SA		Supernatant	
	Stage1	Stage2	Stage1	Stage2	Stage1	Stage2	Stage1	Stage2
CNTs-HFMs (%)	98.78	82.32	77.78	61.43	80.00	--	81.63	58.16
PVDF-HFMs (%)	86.11	59.20	76.79	39.94	52.38	--	68.18	44.73

over, owing to the overlap and interpenetration of CNTs, CNTs-HFMs with mesh-like structures usually present plentiful interconnected pores and high porosities, thus leading to a higher water flux compared with PVDF-HFMs. For example, the flux of CNTs-HFMs and PVDF-HFMs was, respectively, 29.21 and 18.29 L/(m^2·h·bar), 27.25 and 14.17 L/(m^2·h·bar), 16.03 and 12.60 L/(m^2·h·bar) at the end of each stage. Furthermore, the results of flux recovery demonstrated that CNTs-HFMs had a better flux recovery ability. Table 3 shows the percentages of flux recovery at two stages. For HA filtration, the flux of CNTs-HFMs could recover about 98.78% (stage 2) and 82.32% (stage 3), which were all higher than those of PVDF-HFMs (86.11% and 59.20%). According to Fan et al. [36], 98% of flux recovery of CNTs/Al_2O_3 membrane was obtained through coupling with electrochemistry. Katsoufidou et al. [37] studied the anti-fouling ability of ultrafiltration membrane using humic acid; the observed flux recovery rate was about 90% in the first hour. Wei et al. [21] obtained a 85% flux recovery of CNTs-HFMs using the backwash method. In our work, above 98% of flux recovery was obtained by the electrostatic repulsive between CNTs-HFMs membrane surface and negative charged contaminants. Based on the above results, our CNTs-HFMs exhibited a good anti-fouling property compared with the previous studies [21,36-38]. And it was also because the easy hydraulic cleaning can remove most surface deposition compared with the inner fouling.

The above phenomenon can be explained from two aspects, including the nature of HA solution and membrane properties. First, HA is one kind of complexing agent for trace metal elements. HA molecules can be linked together and form large molecular complexes in the presence of Ca^{2+} [39]. The hydrophobic nature of PVDF-HFMs would reject the deposition of high-molecular-weight HA complexes, which results in the external cake layer developing directly on the membrane surface. The layer would be packed down hard and turn to be irreversibly severe fouling gradually with filtering process [40]. Second, the CNTs-HFMs with a good hydrophilicity could form a water layer during the filtering process, which is effective in preventing HA from directly depositing onto the membranes' surface [34,39]. Then it keeps membranes from severe and irreversible fouling, and further benefited for its easy hydraulic cleaning. As several studies described, the membrane fouling control depends on a variety of factors, such as surface charge, surface roughness, surface hydrophilicity, and membrane pore size [29-31]. In this study, experimental results argued for the hydrophilicity as a non-negligible effect on membrane anti-fouling behavior.

Fig. 4(b) shows the flux changes during the whole BSA filtration experiments. The initial flux of CNT-HFMs reached 181.49 L/(m^2·h·bar), more than four-times higher than the initial flux of PVDF-HFMs (40.55 L/(m^2·h·bar)). The flux at the end of each stage was 23.33, 22.30 and 16.72 L/(m^2·h·bar), all of which were higher than those of PVDF-HFMs, (14.64, 9.01 and 6.94 L/(m^2·h·bar)). Obviously, CNTs-HFMs had a better flux recovery ability than that of PVDF-HFMs for BSA filtration, shown in Table 3. Studies revealed that BSA molecules are highly hydrophobic; thus the hydrophobic interaction between the BSA molecules and the membrane surface led to the severely irreversible fouling on PVDF membranes [41]. But the hydrophobic interactions would decrease when abundant hydrophilic functional groups appeared on the CNTs-HFMs. Therefore, the CNTs-HFMs showed an attractive performance with filtering BSA. The other factors for reducing BSA fouling levels were similar to the mechanisms reducing HA fouling [29-31].

In Fig. 4(c), CNTs-HFMs show a superior flux recovery ability and filtration performance for SA than the PVDF at the same conditions. SA molecules with a strong hydrophobic feature were very different with HA and BSA molecules [42]. And with the presence of some metal ions (such as Ca^{2+}) SA and metal ions could produce cross-linked structures and become high molecular weight components. These components can readily accumulate on the membrane surface, resulting in a serious surface fouling [43]. On the other hand, when the hydrophilic SA formed a cake layer on the membrane surface, they would have more recalcitrant resistance to water flow than HA and BSA because of the relatively stronger foulant-water interaction [44,45]. Therefore, both PVDF-HFMs and CNTs-HFMs had a lower flux because of the dense SA cake layer formed. Compared to PVDF-HFMs, the permeability of the modified CNTs-HFMs was enhanced, the irreversible fouling of CNTs-HFMs was drastically mitigated than that of PVDF-HFMs.

The last contaminant was the supernatant of anaerobic bioreactor, which was the mixed solution of low concentration protein, polysaccharide and nucleic acid, etc. [46-49]. It contained the above three pollutants but with relatively much lower concentrations, so the CNTs-HFMs presented an obviously greater anti-fouling performance. Fig. 4(d) depicts a high flux of CNTs-HFMs (about 130 L/(m^2·h·bar)) and a very obvious flux recovery ability, which proved that CNTs-HFMs had a promising filtration performance of supernatant from anaerobic bioreactor. Furthermore, this short-term experiment demonstrated the application potential of CNTs-HFMs in anaerobic bioreactor, which would definitely enhance the stability and prolong the operational period.

3. Filtration Performance of CNTs-HFMs with Voltages

To explore the anti-fouling effect of applying negative voltage on CNTs-HFMs, a negative voltage (−1.0 V) was applied on CNTs-HFMs in the subsequent filtration experiments. Fig. 5 depicts the flux changes by HA, BSA and supernatant of anaerobic bioreactor and SA. Experimental results implied the electrical exclusion effect

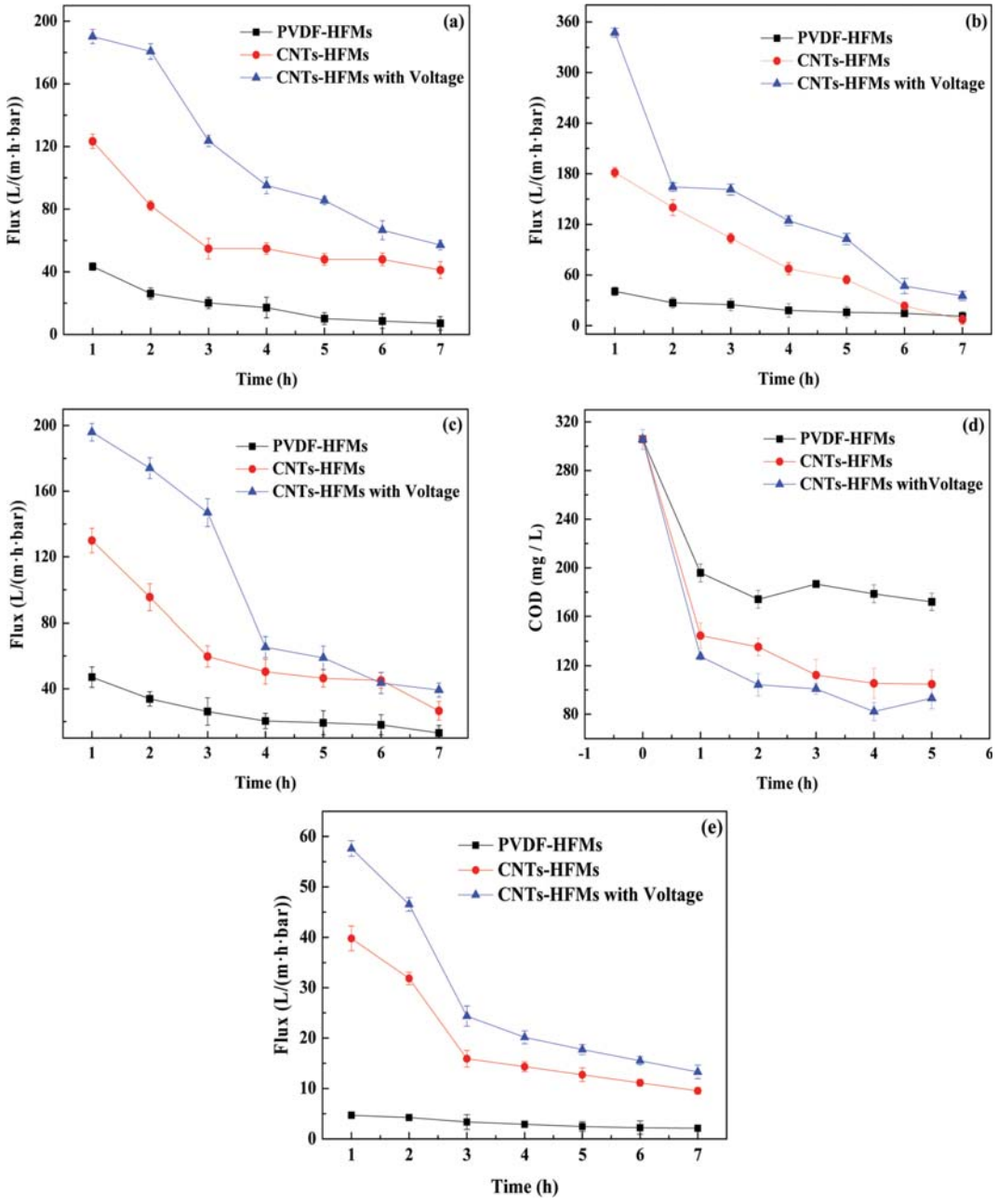

Fig. 5. The flux changes by pollutants: (a) 8 g/L Humic acid; (b) 8 g/L Bovine serum albumin; (c) Supernatant, (e) 4 g/L Sodium alginate and (d) COD changes of supernatant by CNTs-HFMs with voltage, CNTs-HFMs and PVDF-HFMs.

was very noticeable during the whole process. From Fig. 5(a), the fluxes of CNTs-HFMs with negative voltage, CNTs-HFMs without voltage and PVDF-HFM were 190.20, 123.39 and 43.37 L/(m^2·h·bar), respectively, right after 1h filtering HA (8 mg/L). The voltage application improved the flux of CNT-HFMs about 54.1% compared with that without voltage application. While, the flux of CNT-HFMs with voltage was around 4.4-times as high as that of PVDF-HFM. Even at the end of batch filtering tests, the flux of CNTs-HFMs with voltage decreased to 57.06 L/(m^2·h·bar), still much higher than those of CNTs-HFMs without voltage (41.10 L/(m^2·h·bar)) and PVDF-HFM (7.07 L/(m^2·h·bar)). The similar situations were achieved during BSA, SA and supernatant of anaerobic bioreactor filtration, as shown in Fig. 5(b), (c) and (e).

Fig. 5(d) confirms that CNTs-HFMs had also a more effective COD removal performance than that of PVDF-HFMs. The initial COD of anaerobic bioreactor supernatant was 305.7 mg/L, and outlet COD was maintaining about 180 mg/L by PVDF-HFMs filtration, but reduced to 100-140 mg/L after CNTs-HFMs filtration. When applying negative voltage (−1.0 V) on the CNTs-HFMs, the outlet COD decreased impressively to 82 mg/L only by membrane filtering treatment, with an average COD removal rate about 66.8%. When applying a negative voltage, the negative charged pollutant was attracted around the positive electrode region, which would reduce the content of pollutants in the outlet and lead to a rela-

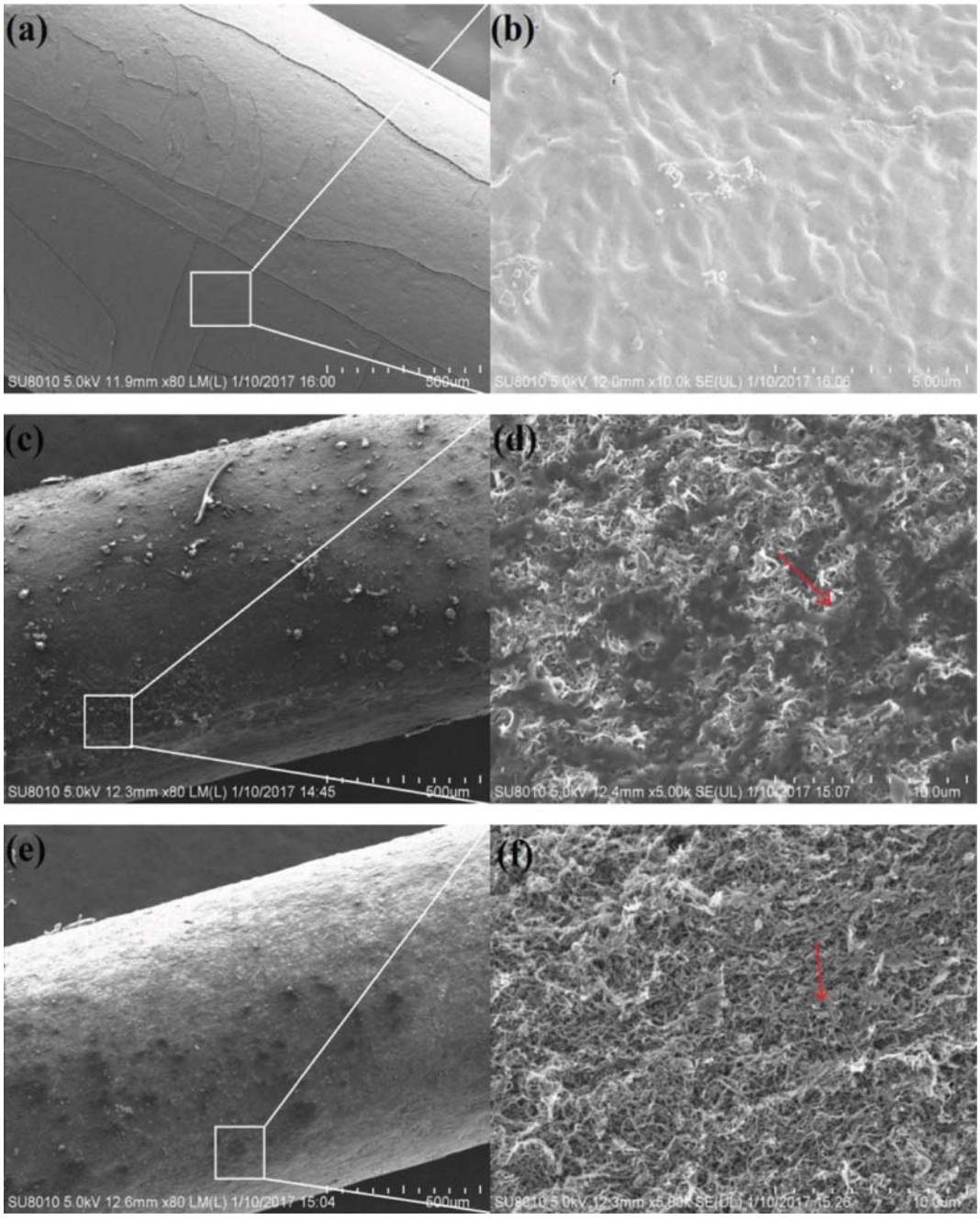

Fig. 6. SEM images with different magnification of membranes surface and cross section by BSA fouling. Surface: (a), (b) PVDF-HFMs; (c), (d) CNTs-HFMs; (e), (f) CNTs-HFMs at "−1.0" voltage. Cross section: (h), (i) CNTs-HFMs; (j), (k) CNTs-HFMs at "−1.0" voltage.

tively low COD. The higher flux than CNTs-HFMs without voltage and PVDF-HFMs can be partially explained by atomic force microscopy observation in the following section.

Combined with SEM images of membrane surface, Fig. 6 demonstrates that the membrane fouling area of PVDF-HFMs (Fig. 6(a), (b)) and CNTs-HFMs without voltage (Fig. 6(c), (d)) was more extensive compared with that of CNTs-HFMs with voltage (Fig. 6(e), (f)). Fig. 6(j), (k) verifies that the contaminant just deposited on the membrane surface of CNTs-HFMs with voltage application, but pollutants blocked membrane inner parts when the membranes were without voltage (Fig. 6(i)). This kind of blockage should be the main reason for severe fouling on the surface of CNT-HFMs without voltage.

4. Interaction Force

A dozen years ago, Li et al. [26] had already used atomic force microscopy (AFM) to unravel the mechanisms of foulant-membrane, foulant-foulant, and foulant-cleaning agent interactions at the molecular level. In this part, a carboxylic polystyrene microparticle was chosen as the probe because carboxylic groups were the predominant function groups of most natural organic pollutants. Each interaction force was measured four times at different positions. Fig. 7 shows the relationship between adhesion force

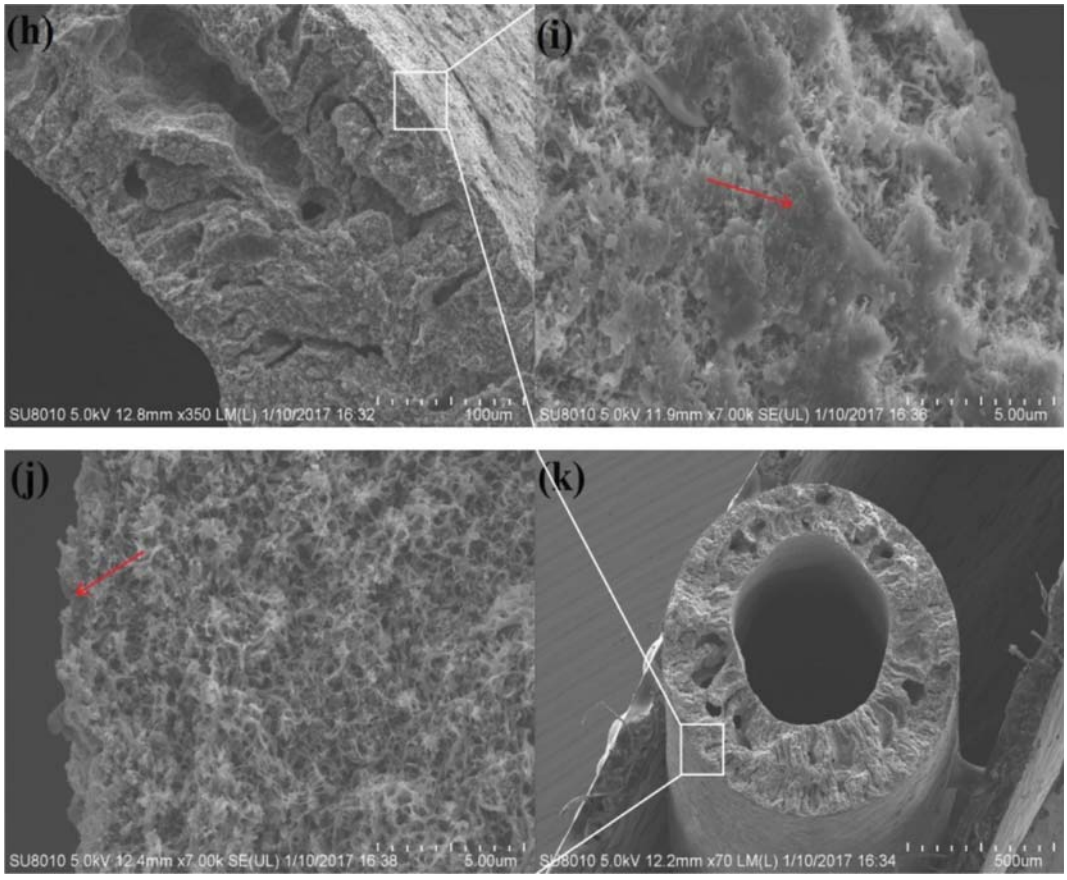

Fig. 6. Continued.

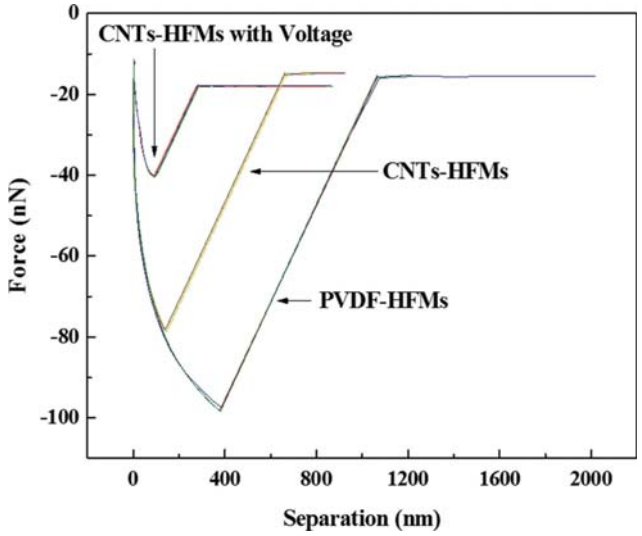

Fig. 7. The interaction force between membranes.

and fracture distance. The adhesion force is the maximum attraction in the interaction force-distance curve, and fracture distance is the distance of the interaction disappears in the interaction force-distance curve. Through both indexes, it could identify the degree of difficulty that membrane fouling occurring and the pollution intensity. According to Fig. 7, the force between membrane and probe (with carboxylic polystyrene micro-particle) was increasing when the probe gradually was away from the membrane surface. And fracture distance would appear when the force suddenly disappeared. From the curve, the adhesion force of CNTs-HFMs with voltage, CNTs-HFMs without voltage and PVDF-HFMs was obtained approximately 36.83, 78.18 and 97.97 nN, respectively. The corresponding fracture distance was 124.04, 145.30 and 380 nm for CNTs-HFMs with voltage, CNTs-HFMs without voltage and PVDF-HFMs. These results corresponded well with our speculation that a strong electrostatic repulsion force can be formed between both negatively charged membrane surface and pollutants [50]. Thus, membrane fouling could be substantially lightened by applying voltage according to obviously reduced interaction force.

CONCLUSIONS

CNTs-HFMs possess several novel properties, such as hydrophilic, smooth surface and interwoven network structures. These characteristics enhance the flux of CNTs-HFMs, when filtering both pure water (average 7-times higher) and natural organic pollutants (average 4.5-times higher) compared with the PVDF-HFMs. Negative voltage application on CNTs-HFMs can form a strong electrostatic repulsion force between negatively charged membrane surface and the pollutants molecules. Therefore, this membrane fouling was alleviated due to the electrostatic repulsion force

imposed by the external electric field, which reduces the deposition of negatively-charged pollutants onto the equally negatively-charged membrane surface. Generally, this work confirmed the potential of electrochemical reinforced CNTs-HFMs for wastewater treatment in anaerobic bioprocess.

ACKNOWLEDGEMENTS

The authors would like to thank the Natural Science Foundation of China (No. 21677026) for financing this research.

SUPPORTING INFORMATION

Additional information as noted in the text. This information is available via the Internet at http://www.springer.com/chemistry/journal/11814.

REFERENCES

1. W. Wang, Q. Yang, S. Zheng and D. Wu, *Bioresource Technol.*, **149**, 292 (2013).
2. Y. An, Z. Wang, Z. Wu, D. Yang and Q. Zhou, *Chem. Eng. J.*, **155**, 709 (2009).
3. Z. Wang, Z. Wu, X. Yin and L. Tian, *J. Membr. Sci.*, **25**, 238 (2008).
4. T. Li, A. W. K. Law, Y. Jiang, A. K. Harijanto and A. G. Fane, *J. Membr. Sci.*, **505**, 216 (2016).
5. I. S. Chang, P. Le Clech, B. Jefferson and S. Judd, *J. Environ. Eng.*, **128**, 1018 (2002).
6. G. Sheng, H. Yu and X. Li, *Biotechnol. Adv.*, **28**, 882 (2010).
7. I. S. Chang and C. H. Lee, *Desalination*, **120**, 221 (1998).
8. K. H. Choo and C. H. Lee, *Water Res.*, **30**, 1771 (1996).
9. R. Chan and V. Chen, *J. Membr. Sci.*, **242**, 169 (2004).
10. W. S. Ang, A. Tiraferri, K. L. Chen and M. Elimelech, *J. Membr. Sci.*, **376**, 196 (2011).
11. A. Al-Amoudi and R. W. Lovitt, *J. Membr. Sci.*, **303**, 4 (2007).
12. N. M. D'souza and A. Mawson, *Crit. Rev. Food Sci.*, **45**, 125 (2005).
13. Z. Wang, J. Ma, C. Y. Tang, K. Kimura, Q. Wang and X. Hang, *J. Membr. Sci.*, **468**, 276 (2014).
14. K. P. Katuri, C. M. Werner, R. J. Jimenez-Sandoval, W. Chen, S. Jeon, B. E. Logan, Z. Lai, G. L. Amy and P. E. Saikaly, *Environ. Sci. Technol.*, **48**, 12833 (2014).
15. P. Gunawan, C. Guan, X. Song, Q. Zhang, S. Su, J. Leong, C. Tang, Y. Chen, M. B. Chan-Park, M. W. Chang, K. Wang and X. Xu, *ACS Nano*, **5**, 10033 (2011).
16. G. L. Wei, X. Quan, S. Chen, X. F. Fan, H. T. Yu and H. M. Zhao, *ACS Appl. Mater. Inter.*, **7**, 14620 (2015).
17. M. Yu, H. H. Funke, J. L. Falconer, R. D. Noble, *Nano Lett.*, **9**, 225 (2008).
18. M. H. O. Rashid, S. Q. T. Pham, L. J. Sweetman, L. J. Alcock, A. Wise, L. D. Nghiem, G. Triani, M. I. H. Panhuis and S. F. Ralph, *J. Membr. Sci.*, **456**, 175 (2014).
19. X. W. Zhang, D. K. Wang, D. R. S. Lopez and J. C. D. da Costa, *Chem. Eng. J.*, **236**, 314 (2014).
20. A. Saxena, B. P. Tripathi, M. Kumar and V. K. Shahi, *Adv. Colloid Interface*, **145**, 1 (2009).
21. G. L. Wei, S. Chen, X. F. Fan, X. Quan and H. T. Yu, *J. Membr. Sci.*, **493**, 97 (2015).
22. Y. K. Wang, W. W. Li, G. P. Sheng, B. J. Shi and H. Q. Yu, *Water Res.*, **47**, 5794 (2013).
23. Z. X. Jin, S. H. Goh, G. Q. Xu and Y. W. Park, *Synthetic Met.*, **135**, 735 (2003).
24. M. D. Frogley, D. Ravich and H. D. Wagner, *Compos. Sci. Technol.*, **63**, 1647 (2003).
25. C. Bower, R. Rosen, L. Jin, J. Han and O. Zhou, *Appl. Phys. Lett.*, **74**, 3317 (1999).
26. Q. Li and M. Elimelech, *Environ. Sci. Technol.*, **38**, 4683 (2004).
27. Q. Li and M. Elimelech, *J. Membr. Sci.*, **278**, 72 (2006).
28. A. Akbari, P. Sheath, S. T. Martin, D. B. Shinde, M. Shaibani, P. C. Banerjee, R. Tkacz, D. Bhattacharyya and M. Majumder, *Nat. Commun.*, **7**, 10891 (2016).
29. V. Vatanpour, M. Esmaeili and M. H. D. A. Farahani, *J. Membr. Sci.*, **466**, 70 (2014).
30. Y. Zhang, Z. Wang, W. Lin, H. Sun, L. Wu and S. Chen, *J. Membr. Sci.*, **446**, 164 (2013).
31. H. Wu, B. Tang and P. Wu, *J. Membr. Sci.*, **428**, 425 (2013).
32. Y. Shimizu, M. Rokudai, S. Tohya, E. Kayawake and T. Yazawa, *Kagaku Kogaku Ronbun.*, **16**, 145 (1990).
33. Z. He, D. J. Miller, S. Kasemset, D. R. Paul and B. D. Freeman, *J. Membr. Sci.*, **525**, 25 (2017).
34. Z. Wang, L. Ci, L. Chen, S. Nayak, P. M. Aiayan and N. Koratkar, *Nano Lett.*, **7**, 697 (2007).
35. B. He, N. A. Patankar and J. Lee, *Langmuir*, **19**, 4999 (2003).
36. X. F. Fan, H. M. Zhao, Y. M. Liu, X. Quan, H. T. Yu and S. Chen, *Environ. Sci. Technol.*, **49**, 2293 (2015).
37. K. Katsoufidou, S. G. Yiantsios and A. J. Karabelas, *J. Membr. Sci.*, **266**, 40 (2005).
38. A. W. Zularisam, A. F. Ismail, M. R. Salim, M. Sakinah and H. Ozaki, *Desalination*, **212**, 191 (2007).
39. J. Tian, M. Ernst, F. Cui and M. Jekel, *Chem. Eng. J.*, **223**, 547 (2013).
40. K. Li, H. Liang, F. Qu, S. Shao, H. Yu, Z. Han, X. Du and G. Li, *J. Membr. Sci.*, **471**, 94 (2014).
41. A. E. Contreras, A. Kim and Q. Li, *J. Membr. Sci.*, **327**, 87 (2009).
42. H. C. Kim and B. A. Dempsey, *J. Membr. Sci.*, **428**, 190 (2013).
43. M. Hashino, T. Katagiri, N. Kubota, Y. Ohmukai, T. Maruyama and H. Matsuyama, *J. Membr. Sci.*, **366**, 258 (2011).
44. F. Qu, H. Liang, Z. Wang, H. Wang, H. Yu and G. Li, *Water Res.*, **46**, 1490 (2012).
45. L. Bai, H. Liang, J. Crittenden, F. Qu, A. Ding, J. Ma, X. Du, S. Guo and G. Li, *J. Membr. Sci.*, **492**, 400 (2015).
46. H. Ryssov-Nielsen, *Vatten*, **1**, 33 (1975).
47. J. T. Novak, A. Zurow and H. Becker, *J. Environ. Eng. Div.*, **103**, 815 (1977).
48. S. Kang, M. Kishimoto, S. Shioya, T. Yoshida, K. Suga and H. Taguchi, *J. Ferment. Bioeng.*, **68**, 117 (1989).
49. H. C. Flemming and J. Wingender, *Water Sci. Technol.*, **43**, 1 (2001).
50. V. Vatanpour, S. S. Madaeni, R. Moradian, S. Zinadini and B. Astinchap, *J. Membr. Sci.*, **375**, 284 (2011).

Supporting Information

Anti-fouling characteristic of carbon nanotubes hollow fiber membranes by filtering natural organic pollutants

Yue Yang, Sen Qiao†, Ruofei Jin, Jiti Zhou, and Xie Quan†

Key Laboratory of Industrial Ecology and Environmental Engineering (Ministry of Education, China), School of Environmental Science and Technology, Dalian University of Technology, Dalian 116024, P. R. China
(*Received 22 September 2017 • accepted 26 December 2017*)

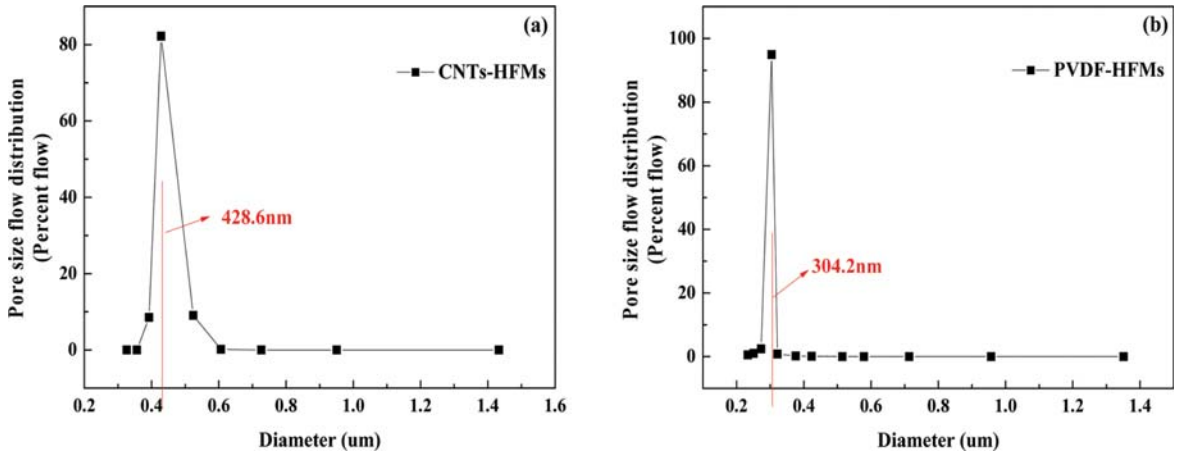

Fig. S1. The pore size of CNTs-HFMs (a) and PVDF-HFMs (b).

Table S1. Characteristics of the CNT membrane in the literatures

	$CNTs/Al_2O_3$ membrane	CNTs/ceramic membrane	CNT hollow-fiber membranes	This work
Materials	$CNTs/Al_2O_3$	CNTs/ceramic	CNTs	CNTs
Pore size (nm)	171	150	100	429
Voltage (V)	+1.5	Alternating polarization	1.5	−1.0
Target object	Humic acid	Humic acid	Gold nanoparticles	Humic acid Bovine serum albumin, Sodium alginate Supernatant of anaerobic bioreactor COD
Removal (%)	87.7	76	86	67
Highest flux recovery rate (%)	98	——	85	98.78

Table S2. Characteristics of single PVDF-HFM and CNT-HFM

Parameters	PVDF-HFM	CNT-HFM
Outer/inner diameter	400/240 μm	1600/690 μm
Pore size	304.2 nm	428.6 nm
Pure water flux (0.7 bar)	44.1 $L/m^2 \cdot h$	339.49 $L/m^2 \cdot h$
Contact angle	Average 102.26°	Average 75.36°
Structure	Finger-like macrovoids and sponge-like substructure	Interwoven network structure

REFERENCES

1. X. F. Fan, H. M. Zhao, Y. M. Liu, X. Quan, H. T. Yu and S. Chen, *Environ. Sci. Technol.*, **49**, 2293 (2015).
2. X. F. Fan, H. M. Zhao, X. Quan, Y. M. Liu and S. Chen, *Water Res.*, **88**, 285 (2016).
3. G. L. Wei, S. Chen, X. F. Fan, X. Quan and H. T. Yu, *J. Membr. Sci.*, **493**, 97 (2015).